Using track-elasticity for noise mitigation on low-vibration track

Jannik Theyssen, Astrid Pieringer, Wolfgang Kropp

Division of Applied Acoustics, Chalmers University of Technology, Gothenburg, Sweden, Email: jannik.theyssen@gmail.com

Introduction

Ballasted tracks feature a two-stage elastic support, with the ballast layer and the rail pad both contributing to the vertical and lateral track elasticity. Many common slab track systems replace the two-stage elastic support with a one-stage elastic support, requiring a comparatively softer rail pad [1]. The resulting decoupling of the rail from its support leads to higher vibration levels in the rail and consequentially to higher levels of airborne noise radiation from the rail [2].

Increasing the rail pad stiffness is usually not a viable option on slab track systems with a single stage elastic support as this increases the stress on the track components, leading to higher rates of wear and possibly damage. Further, the transfer of vibrational energy into the slab and ground could increase ground vibrations and noise. However, slab track systems with a two-stage elastic support exist, such as systems with booted sleepers. The low-vibration track [3], which is often found in tunnels due to its vibration isolation properties, is such a track. The aim of this work is to explore, starting from the standard parameters of the low-vibration track, the implications of changing the rail pad stiffness and boot stiffness for the receptance, radiated sound power, slab vibrations and rolling contact forces. It should be noted that the work is conducted independent of a specific track manufacturer and in principal, the method can be translated to any track with a two-stage elastic support.

Method

The modelling of the dynamic response and the radiation from the railway track is carried out numerically. The dynamic model of the track is consists of numerical models for the rail and the slab layers, as well as an analytical model for the sleeper response. The rail and the slab are modelled using the Waveguide Finite Element method [4]. This method makes use of the waveguide properties of long structures such as the rail and the slab by assuming propagating, decaying waves along the length of the structure. Thus, only the cross-section of the structure is discretized, allowing a computationally efficient solution of the finite element problem. The calculated transfer functions to any point on the structure include the complex interaction of all relevant wave types.

The rail has a standard rail geometry with a weight of 60 kg/m. The discretization of the cross-section is shown in Figure 1. The validated model for the dynamic slab track response is described in [5]. Half of its symmetric geometry is shown in Figure 2. Both the rail and the slab use 9-node quadrilateral elements with quadratic shape functions.

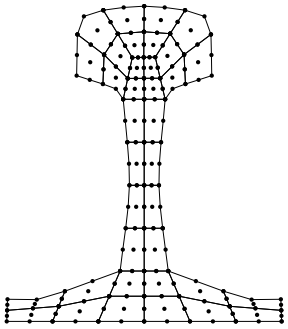

Figure 1: Discretized cross-section of the rail geometry.

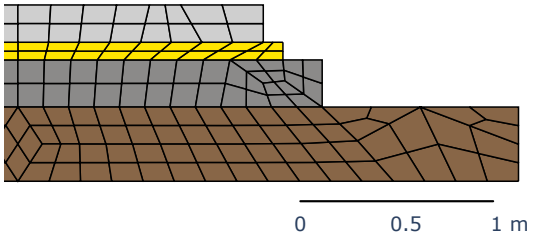

Figure 2: Discretized cross-section of the slab track geometry, with (top to bottom) the pre-stressed concrete slab, an adjustment layer, a concrete base layer and the ground. The ground layer has a fixed boundary condition at its base.

The two waveguides, rail and slab, are coupled via spring-mass-spring systems in 99 locations, where the springs and masses are modelled as linear, lumped elements. Damping is included in the springs using complex loss factors. The ground receptance below the track support layers is included in the WFE model. A principal setup of the model is shown in Figure 3. The coupling is carried

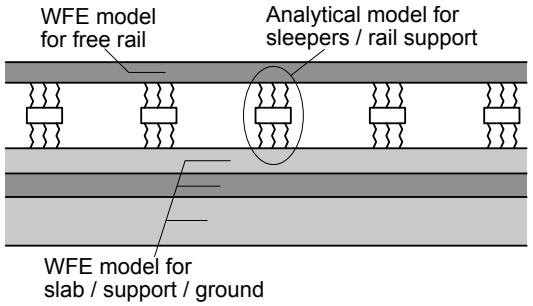

Figure 3: Principal sketch of the combined model for rail, sleepers and slab track.

out by evaluating the transfer functions in the waveguides from all coupling positions to all coupling positions and formulating a linear system of equations, which can be solved for the reaction forces in the pads and sleeper boots, comparable to [6, 5]. The connection forces can

then be used to determine the surface velocity at any point on the rail and slab surface for a harmonic unit excitation, as well as the sleeper vertical and lateral velocity. The point receptance at the top of the rail calculated using the model is used to compare different track setups and serves as the input to a time-domain calculation of the wheel-rail interaction forces. Further, the model is used to compare the track decay rates of the different tracks.

Finally, the surface normal vibration of the three components rail, sleepers and slab produced using the dynamic track model serve as the input to a Boundary Element (BE) model, likewise formulated in the frequency-wavenumber domain. This wavenumber-domain BE model includes the surface vibrations from all components and thus takes into account their acoustic coupling [4, 7].

Four combinations of the two elasticities are compared as summarized in Table 1. The central mass of the sleeper

Table 1: Vertical stiffness of rail pad and boot in the four different cases.

	A	B	C	D
Rail pad (kN/mm)	100	200	400	800
Boot (kN/mm)	40	33.5	31	30

is set to 99 kg in all cases. This way, the first track setup closely resembles the properties of a track that is in operation in the Swiss railway network. The other three cases were generated by multiplying the rail pad stiffness with a factor of two and adjusting the boot stiffness such that the static stiffness of the series of springs k_{tot} remains roughly constant,

$$\frac{1}{k_{\mathrm{tot}}} \stackrel{!}{=} \frac{1}{k_{\mathrm{p,i}}} + \frac{1}{k_{\mathrm{b,i}}} \tag{1}$$

with i representing case A, B, C, or D.

Results

The total vertical track receptance is shown in Figure 4. It is clear the the track receptance is almost identical for all cases up to about 100 Hz. Four relevant resonances occur in the track in vertical direction below 1 kHz, this being (I) the resonance at which the whole slab is moving up and down ($f0$) typically below 50 Hz, determined by the mass of the slab and the ground stiffness, (II) the resonance of the sleepers on the slab $f1$ at around 100 Hz and determined mostly by the boot stiffness, (III) the antiresonance at which the sleeper vibrates out of phase with the slab and the rail, effectively acting as a dynamic absorber for the rail vibration, and (IV) the resonance of the rail on the sleepers $f3$, which is largely determined by the rail pad stiffness. The largest differences in the track receptance are observed between 150 Hz and about 1 kHz, between $f1$ and $f3$. The increased track stiffness and with that, the stiffer coupling of the rail to the sleepers expectedly leads to an increase of the track decay rate as shown in Figure 5. A distinct increase in the TDR can be observed above 250 Hz and up to 4 kHz, which covers the frequency range relevant for the noise radiation

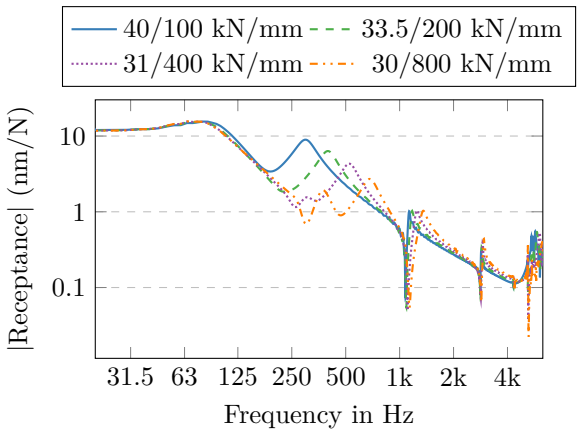

Figure 4: Total vertical track receptance for the different cases, with the excitation above a sleeper.

from the rail. Based on this, a decrease of the radiated

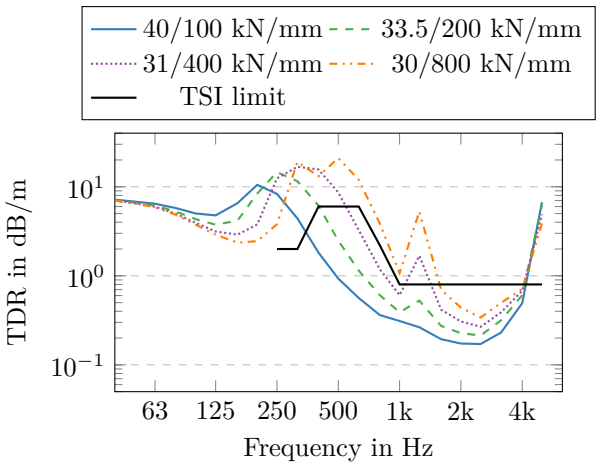

Figure 5: Comparison of the track decay rate cases A to D.

sound power is expected. Figure 6 shows the total sound power radiated by the track for the different track setups for harmonic unit excitation, as well as the differences of cases B to D relative to case A. Significantly decreased sound pressure levels are observed above about 250 Hz, where a decrease of about 10 dB is seen up to about 2 kHz. An increase in the radiated sound power can be observed at 63 Hz and around 200 Hz.

An investigation into the contribution of each component to the total radiated sound power shows that in the frequency regions with an increased radiation, the slab and the sleeper are the dominant noise sources. The individual contributions for case A and D are shown in Figure 7. The slab vibration is the dominant noise source below about 80 Hz to 125 Hz, depending on the setup. Above that, the sleepers take over and dominate the spectrum up to about 300 Hz to 600 Hz. With stiffer rail pads, the frequency up to which the sleepers are dominant is shifted up because of both the increased sleeper vibration as well as the decreased rail vibration. For higher frequencies, the rail dominates the sound power spectrum.

As low-vibration tracks are often used in situations where

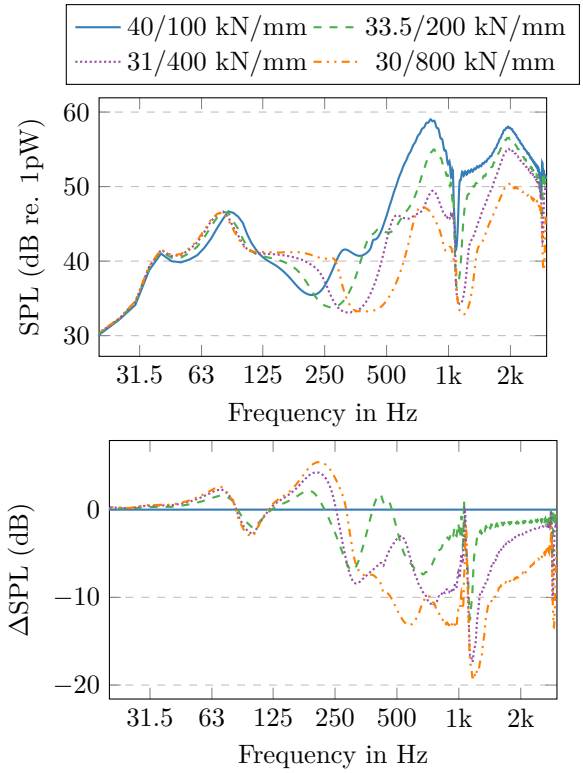

Figure 6: Total sound power radiated by each track for a harmonic unit force excitation.

ground-borne vibration isolation is of concern, a comparison of the slab vibration is relevant. Figure 8 shows the insertion loss, a comparison of the transfer receptance for an excitation on the top of the rail to the slab centre position. Up to about 80 Hz, no large difference is observable. The lowered boot stiffness leads to an increased vibration isolation up to 10 dB in the frequency range up to about 300 Hz. Above about 400 Hz, the slab surface vibrates up to 20 dB more for case D compared to case A. However, this frequency range is not typically considered relevant for ground-borne vibration and noise [8, 9].

The in-house software WERAN [11] was used to evaluate the influence of the changed track stiffness on the rolling contact forces. This time-domain simulation discretises the contact patch and solves the interaction of wheel and rail based on moving Green's functions. A train speed of 100 km/h and a pre-load of 55 kN were assumed. The identical combined roughness of wheel and rail as well as the wheel response is used in all cases to make the results comparable. Finally, an auto-spectrum of the calculated time-history in third-octave bands of contact forces is generated and shown in Figure 9. Changing the track parameters affects the contact forces mainly in the frequency range between 50 Hz and 1.2 kHz. While for stiffer pads an increase of up to 6 dB is observed in the 250 Hz third-octave band, a decrease of about 4 dB can be seen in the 630 Hz band. Comparing this to Figure 4, it is clear that generally, higher forces in the rolling contact are found in frequency regions with a decreased track receptance due to the stiffer rail pads.

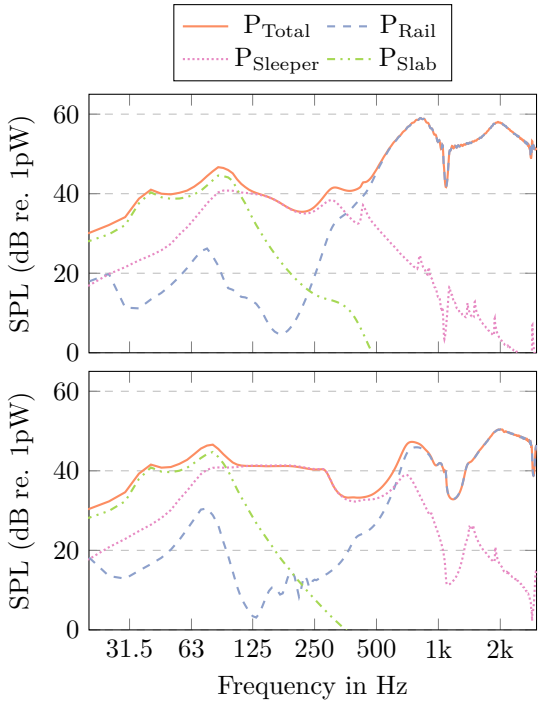

Figure 7: Contributions of individual track components to the overall sound power. Top: Case A, Bottom: Case D.

Discussion and Conclusion

A short discussion of excluded research, an outlook on open questions and a summary are given in the following. This study neglects the influence of the radiation from the wheel. As seen, the contact force spectra change, and with an increased contact force, an increased radiation from the wheel should be expected. However, this study suggests that for the given changes in the track stiffness, the forces mainly increase below 400 Hz. Typically, railway wheels do not have a high radiation efficiency in this frequency range [2, 10], and thus no large differences are expected in this context.

In the future, this study could be extended to ballasted tracks by including under-sleeper pads. This way, combinations of the stiffness above and below the sleeper can be produced analogously to the method shown above,

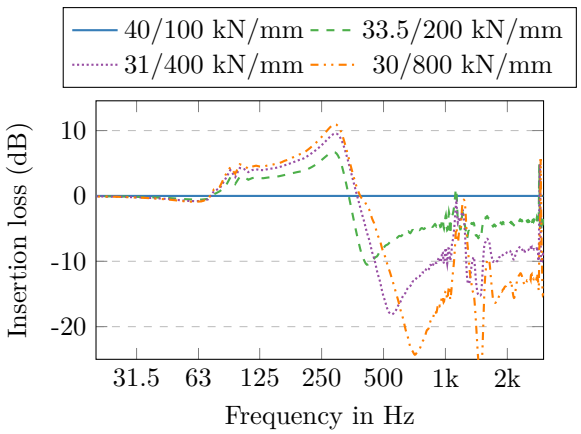

Figure 8: Insertion loss, comparing slab track surface vibrations for Cases B to D to case A.

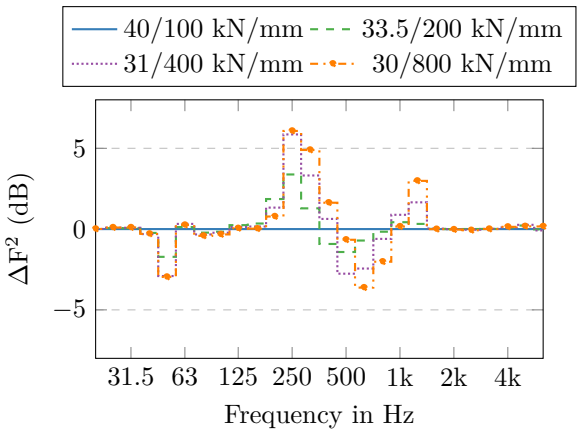

Figure 9: Autospectra of the rolling contact force.

similarly to the approach used in the article by Diehl et al. [12]. Further, the use of rail pads with higher damping coefficients can be explored in this context. By providing a stronger coupling between the rail and the sleeper, rail pads with high loss factors can use their full potential. The influence of the lateral stiffness has been neglected in this study, as the construction of the sleeper boot has the primary goal of providing an extra elasticity in the vertical direction.

Increasing the rail pad stiffness is a known method to reduce the rolling noise radiated from the rail. However, a studies of the noise reduction often neglect the disadvantages of this method, namely the increased groundborne vibration, stresses on the components, and increased rolling contact forces. This study quantifies the effects on these related issues while providing a possible solution for a specific type of slab track. Increasing the rail pad stiffness while reducing the stiffness below the booted sleeper reduces the radiation from the rail while it maintains or increases the ground borne vibration isolation up to about 300 Hz. An increased sound radiation from the sleepers of up to 6 dB is observed at the sleeper resonance.

Acknowledgements

The current study is part of the ongoing activities in CHARMEC - Chalmers Railway Mechanics (www.charmec.chalmers.se). Parts of the study have been funded from the European Union's Horizon 2020 research and innovation programme in the In2Track3 project under grant agreements No 101012456. The computations were enabled by resources provided by the Swedish National Infrastructure for Computing (SNIC), partially funded by the Swedish Research Council through grant agreement no. 2018-05973.

References

[1] Gautier, P.-E.: Slab track: Review of existing systems and optimization potentials including very high speed. Construction and Building Materials (2015), 92, 9–15.

[2] Thompson, D. J.: Railway noise and vibration: Mechanisms, modelling and means of control, Elsevier, 2009.

[3] Sonneville, Low-vibration track, URL: `https://www.sonneville.com/low-vibration-track-lvt`, Accessed 2022-03-29.

[4] Nilsson, C.-M., Jones, C. J. C., Thompson, D. J., and Ryue, J.: A waveguide finite element and boundary element approach to calculating the sound radiated by railway and tram rails. Journal of Sound and Vibration, 321(3–5) (2009), 813–836

[5] Theyssen, J. S., Aggestam, E., Zhu, S., Nielsen, J. C. O., Pieringer, A., Kropp, W., and Zhai, W.: Calibration and validation of the dynamic response of two slab track models using data from a full-scale test rig. Engineering Structures (2021), 234, 111980.

[6] Zhang, X., Thompson, D. J., Li, Q., Kostovasilis, D., Toward, M. G. R., Squicciarini, G., and Ryue, J.: A model of a discretely supported railway track based on a 2.5D finite element approach, Journal of Sound and Vibration (2019), 438, 153–174.

[7] Theyssen, J. S., Pieringer, A., and Kropp, W.: The Influence of Track Parameters on the Sound Radiation from Slab Tracks. In G. Degrande, G. Lombaert, D. Anderson, P. de Vos, P.-E. Gautier, M. Iida, J. T. Nelson, J. C. O. Nielsen, D. J. Thompson, T. Tielkes, and D. A. Towers (Eds.), Noise and Vibration Mitigation for Rail Transportation Systems (Vol. 150, pp. 90–97), 2021. Springer International Publishing.

[8] Hemsworth, B: REDUCING GROUNDBORNE VIBRATIONS: STATE-OF-THE-ART STUDY, Journal of Sound and Vibration (2000), 231(3), 703–709.

[9] Ntotsios, E., Thompson, D. J., and Hussein, M. F. M.: A comparison of ground vibration due to ballasted and slab tracks. Transportation Geotechnics (2019), 21, 100256.

[10] Fabre, F., Theyssen, J. S., Pieringer, A., and Kropp, W.: Sound radiation from railway wheels including ground reflections: A half-space formulation for the Fourier boundary element method. Journal of Sound and Vibration (2021), 493, 115822

[11] A. Pieringer, W. Kropp, D. Thompson, Investigation of the dynamic contact filter effect in vertical wheel/rail interaction using a 2D and a 3D non-Hertzian contact model, Wear 271 (2011) 328â€“338

[12] Diehl, R. J., Nowack, R., and Hoelzl, G.: SOLUTIONS FOR ACOUSTICAL PROBLEMS WITH BALLASTLESS TRACK, Journal of Sound and Vibration (2000), 231(3), 899–906